

1 **Collagen prolyl hydroxylation-dependent metabolic perturbation governs**
2 **epigenetic remodeling and mesenchymal transition in pluripotent and cancer**
3 **cells**

4
5 Cristina D'Aniello^{1,4}, Federica Cermola^{1,4}, Andrea Palamidessi², Luca G. Wanderlingh^{3,†}, Miriam
6 Gagliardi⁴, Agnese Migliaccio¹, Francesca Varrone³, Laura Casalino^{1,4}, Maria R. Matarazzo⁴,
7 Dario De Cesare^{1,4}, Giorgio Scita^{2,5}, Eduardo J. Patriarca^{1,4*}, Gabriella Minchiotti^{1,4*}

8
9 ¹ Stem Cell Fate Laboratory, Institute of Genetics and Biophysics, 'A. Buzzati-Traverso', CNR,
10 80131 Naples, Italy.

11 ² IFOM, the FIRC Institute of Molecular Oncology, 20139 Milan, Italy

12 ³ IRBM, 80131 Naples, Italy.

13 ⁴ Institute of Genetics and Biophysics, 'A. Buzzati-Traverso', CNR, 80131 Naples, Italy.

14 ⁵ University of Milan, Department of Oncology and Hemato-Oncology.

15 †Current address: Telethon Institute of Genetics and Medicine (TIGEM), Pozzuoli, Naples, Italy.

16
17 *Correspondence to:

18 Gabriella Minchiotti: Via Pietro Castellino 111, 80131 Naples, Italy; +390816132357;
19 gabriella.minchiotti@igb.cnr.it

20 Eduardo J. Patriarca: Via Pietro Castellino 111, 80131 Naples, Italy; +390816132431;
21 eduardo.patriarca@igb.cnr.it

22
23 **Running title:** Metabolic control of cell state transition dynamics

24 **Conflict of Interest:** "The authors declare no potential conflicts of interest"

1 **Abstract**

2 Collagen prolyl hydroxylation (CPH), which is catalyzed by prolyl 4-hydroxylase (P4H), is the
3 most prevalent posttranslational modification in humans and requires Vitamin C (VitC). Here we
4 demonstrate that CPH acts as an epigenetic modulator of cell plasticity. Increased CPH induced
5 global DNA/histone methylation in pluripotent stem and tumor cells and promoted cell state
6 transition (CST). Interfering with CPH by either genetic ablation of P4H subunit alpha-2
7 (P4HA2) or pharmacologic treatment reverted epigenetic changes and antagonized CST.
8 Mechanistically, we suggest that CPH modifies the epigenetic landscape by reducing VitC for
9 DNA and histone demethylases. Repurposed drugs targeting CPH-mediated metabolic
10 perturbation, such as the antiasthmatic Budesonide, blocked metastatic dissemination of breast
11 cancer cells in vivo by preventing mesenchymal transition. Our study provides mechanistic
12 insights into how metabolic cues and epigenetic factors integrate to control cell state transition
13 and paves the way for the development of novel antimetastatic strategies

14

15 **Significance:** A phenotype-based HTS reveals unforeseen metabolic control of cell plasticity and
16 identifies Budesonide as a drug candidate for metastatic cancer

17

18 **Keywords:** P4HA2, Vitamin C, Fe⁺²/αKG -dependent dioxygenases, DNA methylation,
19 pluripotent stem cells, cancer cells, cell state transition, metastasis, drugs repurposing,
20 Budesonide

21

1 **Introduction**

2 Cell plasticity is the ability of cells to switch between different phenotypic states in a reversible
3 manner. Besides its crucial role in the development of multicellular organisms and tissue
4 homeostasis, cell plasticity contributes to the progression of devastating pathologies, including
5 metastatic cancer and organ fibrosis (1-3). The primary source of cell plasticity is the Epithelial-
6 Mesenchymal Transition (EMT). EMT is not an all-or-none, irreversible process, as cohesive
7 epithelial cells and free motile/migrating mesenchymal cells represent only the extreme of a
8 continuum of intermediate/metastable phenotypes. How cell state transition is controlled and
9 what are the molecular determinants that enable cells to reside stably in one or another
10 phenotypic state is a major unresolved issue (2, 4). Transient metabolic perturbations that modify
11 the availability of epigenetic enzymes required metabolites (EEMs) are emerging as candidate
12 determinants of cell plasticity (5). Typical examples are the ascorbic acid [Vitamin C (VitC)] and
13 the alpha-ketoglutarate (α KG) that are cofactors/enhancers for the Fe^{+2}/α KG -dependent
14 dioxygenases superfamily (6), which include the Ten-Eleven Translocation (TET) DNA
15 demethylases and the Jumonji (JMJ) domain-containing histone demethylases. VitC, for
16 instance, by enhancing the activity of the TET and JMJ demethylases, improves the efficiency of
17 induced pluripotent stem cell (iPSC) generation (7-10), drives embryonic stem cells (ESCs)
18 towards a naive state of pluripotency (11, 12) and regulates the balance between self-renewal and
19 differentiation of hematopoietic stem cells (13, 14). Thus, fluctuation of EEMs' concentrations is
20 considered an additional layer of epigenetic regulation (15). Yet, how this is regulated is still
21 unknown. Here, we reveal that VitC -consuming collagen prolyl hydroxylases (P4Hs), which
22 catalyze the hydroxylation of prolyl residues on nascent collagens, are key players in this
23 complex regulatory scenario. Specifically, through an unbiased phenotype-based screening of

1 1.200 FDA-approved drugs, we identify compounds that are used to gain insight into unexplored
2 molecular mechanisms of cell plasticity, and as drugs to target diseases associated with cell state
3 transition, most and foremost cancer progression and metastatic dissemination.

4

1 **Materials and Methods**

2 **Cell lines, culture conditions and treatments**

3 SUM159 cells were from Asterand (2015), and A549 cells were from NIH NCI-60 cell line panel
4 (2011) and their identity and mycoplasma free-state is routinely (annually) tested by DNA
5 fingerprinting using Short tandem repeat (STR) profiling, and by PCR-based, MycoAlert™
6 Mycoplasma Detection Kit (Lonza, Bioscience). Each cell lines were used within passage 4/5
7 since their thawing from originally frozen vials.

8 A549 cells were cultured in high glucose DMEM (Invitrogen, Life Technologies), 10% FBS
9 (Euroclone), 2 mM glutamine and penicillin/streptomycin (100 U/ml, GIBCO). SUM-159 cells
10 were cultured in F12 medium with inactivated calf serum (5%), 10 mM Hepes, 1 ug/ml
11 hydrocortisone (HYC), insulin (5ug/ml), and penicillin/streptomycin. For quantification of
12 collagen and Collagen-Hydroxyproline (C-HyP), and histone methylation, WT SUM159 cells
13 were starved of HYC for 48hrs and then treated with HYC ± Budesonide (25µM) for 48 hours.

14 Wild-type TBV2 (129/SvP) were kindly provided by Dr. Stefania Filosa in 2008, *P4ha2^{KO}* and
15 *P4ha2^{KO}/P4ha1^{KD}* TBV2 mouse ESCs were maintained as reported (16); mycoplasma free-state
16 is routinely (twice/year) tested by PCR-based assay. All the experiments were performed
17 between the 5th and the 20th cell passage.

18 L-Pro-induced esMT was performed as described (16). Briefly, ESCs (250 cells/cm²) were plated
19 onto gelatin-coated plates in ESC medium (DMEM/10%FBS/LIF) ± L-Pro (500 µM - 1 mM) for
20 5 days. Medium was renewed at day 3 with addition of fresh L-Pro.

21 PiC to ESC reverse transition (MesT) was performed as described (16). VitC (Sigma-Aldrich)
22 was dissolved in water. CHIR99021 was dissolved in DMSO and used at 3 µM (Millipore).

1 EsMT inhibitors (Sigma-Aldrich) were dissolved in DMSO at 10 mM and used at concentration
2 ranging from 5 to 20 μ M.

3 The Alkaline phosphatase (AP) assay was performed using AP staining kit (System Biosciences)
4 following manufacturer's instructions.

5 For Collagen and C-HyP quantification, ESCs (15×10^3 /cm²) or PiCs (15×10^3 /cm²) were plated
6 in gelatin and treated \pm L-Pro and \pm Budesonide and VitC. After 48hrs in culture, cells were
7 collected and analyzed either by WB or immunofluorescence (see below for details).

8

9 **High-throughput screening**

10 The Prestwick Chemical Library® 1200 compounds ([www.prestwickchemical.com/libraries-](http://www.prestwickchemical.com/libraries-screening-lib-pcl.html)
11 [screening-lib-pcl.html](http://www.prestwickchemical.com/libraries-screening-lib-pcl.html)) was used for the screening. The screening was performed using the
12 *Cell^{maker}* robotic platform (16). TBV2 ESCs were plated at 250 cells/cm² in gelatin-coated plates
13 (96-multiwell) in DMEM/10%FBS/LIF. Five hours after plating, cells were supplemented with
14 L-Pro (250 μ M) or left untreated as control, and the compounds (Prestwick chemical library®)
15 were singularly added at a final concentration of 10 μ M. At day 4 after treatment, the resulted
16 colonies were fixed/stained in PBS1x/6% glutaraldehyde/0.15% crystal violet for 30 min at RT.
17 The plates were scanned/imaged and the cell colonies (if any) were analyzed using the ImageJ
18 1.46r software (<http://image.nih.gov/ij>).

19 Chemical structure information for Budesonide are available at [Pubchem
20 (<https://pubchem.ncbi.nlm.nih.gov/compound/5281004>), DrugBank(<https://www.drugbank.ca/drugs/DB01222>) and Therapeutic Target Database (<https://db.idrblab.org/ttd/drug/d0y7iu>).

22

1 **RNA extraction and quantitative RT-PCR**

2 Total RNAs were extracted using the RNeasy kit (Quiagen) and reverse transcribed with the
3 QuantiTect Reverse Transcription kit (Qiagen). qPCR was performed using SYBR Green PCR
4 master mix (FluoCycle IITM SYBR, EuroClone). Primers are listed in Table S1.

6 **Cell proliferation assays**

7 Cell proliferation was evaluated using FACS- based EdU incorporation (Click-iT® EdU Flow
8 Cytometry Assay kit; Molecular Probes), and the CCK-8 (Dojindo Laboratories, Kumamoto,
9 Japan) assays following manufacturer instructions.

11 **Western blot**

12 Total proteins were extracted in 100 mM Tris pH 8, 140 mM NaCl, 20 mM EDTA, 0,2% SDS,
13 1% Nonidet P-40 lysis buffer, resolved on SDS-PAGE gels and transferred onto PVDF
14 membranes (iBlot dry Transfer System; Life Technologies).

15 Histones proteins were prepared as follows: cell pellets were resuspended in Triton Extraction
16 Buffer (TEB: PBS containing 0.5% Triton X 100 (v/v), 2mM phenylmethylsulfonylfluoride
17 (PMSF), 0.02% (w/v) NaN₃) at a cell density of 10⁷ cells per ml. Then, the pellets were lysed
18 overnight in 0,2N HCl at a density of 4x10⁷ cells/ml.

19 Primary Antibodies (listed in Table S2) were used overnight at 4°C followed by the appropriate
20 HRP-conjugated secondary antibodies. Detection was performed with ECL reagents (Pierce,
21 Thermo Scientific). ImageJ software was used for the densitometric analysis.

22

23 |

1 **Immunofluorescence analysis and quantification**

2 Cells were fixed (4% PFA) and permeabilized (0.1% Triton X-100) for 10 minutes at RT and
3 incubated with blocking solution (0.1% Triton X-100/5% BSA) for 1 hrs. Primary Antibodies
4 (listed in Table S2) were incubated overnight (4°C) followed by the relative secondary
5 antibodies (Alexa Fluor Molecular Probes)

6 Images were obtained using the DMI6000B microscope equipped with DFC 350FX B/W digital
7 camera (Leica Microsystems). Confocal images were obtained on a Nikon A1 microscope. The
8 AF6000 (Leica Microsystems) and NIS Element C (Nikon, Tokyo) software were used for image
9 acquisition/elaboration.

10 For cytopsin samples, dissociated cells were resuspended in 15% FBS/1x PBS and centrifuged at
11 800 rpm for 8 min using a Thermo Shandon Cytocentrifuge (CytoSpin™ 4), and fixed for
12 further analysis.

13 C-HyP positive area (pixel/cm²) was measured over the total nuclei area (100-300
14 cells/conditions) using ImageJ software ([https://imagej.nih.gov/ij/docs/guide/146-30.html#toc-](https://imagej.nih.gov/ij/docs/guide/146-30.html#toc-Subsection-30.2)
15 [Subsection-30.2](https://imagej.nih.gov/ij/docs/guide/146-30.html#toc-Subsection-30.2))

16

17 **Generation of *P4ha2*^{KO} and *P4ha2*^{KO}/*P4ha1*^{KD} ESCs and tumor cells**

18 For CRISPR/Cas9 mediated *P4ha2* knock-out, TBV2 ESCs were infected with lentiviral
19 particles (1 MOI) carrying the guide RNA (gRNA), which targets *P4ha2* exon 6
20 (ATCCGGACACGATTTCCAGA) followed by the Cas9 and the Puromycin resistance
21 [transEDIT™ Lentiviral gRNA plus Cas9 (pCLIP-All) Target Gene; transOMIC technologies].

22 Following Puromycin selection (1 µg/ml; 6 days), resistant cells were dissociated and single cells
23 were FACS-sorted (FACS Aria, Becton Dickinson) on the basis of FSC/SSC parameters and

1 seeded into 96-well plates. Genomic DNA was analyzed by PCR using primers designed on
2 intron 5-6 (forward) and 6-7 (reverse) sequences that amplify a product of 735 bp. IN/DEL
3 mutations were identified by digesting PCR products with the T7 endonuclease and confirmed
4 by sequencing. The absence of the wild type allele was confirmed by RT-PCR (see Table S1).

5 *P4ha2^{KO}/P4ha1^{KD}* ESCs were obtained by transfecting *P4ha2^{KO}* ESCs (Clone #1) with short
6 hairpin RNAs (shRNAs) plasmids targeting different non-overlapping *P4ha1* mRNA sequences
7 followed by a GFP reporter (shERWOOD UltramiR Lentiviral shRNA, pZIP-mEF1a,
8 TransOMIC). 48hrs after electroporation single GFP positive cells were FACS sorted into 96-
9 well plates, and analyzed as above.

10 Stable *P4HA2^{KD}* A549 and SUM159 cells were generated by lentiviral infection of shRNAs
11 (PLKO, SIGMA) followed by Puromycin selection (1 μ g/ml; 10 days).

12

13 **Quantification of 5hmC**

14 Gelatin plated ESCs (15×10^3 /cm²) were pre-treated with VitC (50 μ M; 24 hrs) before addition of
15 L-Pro \pm Budesonide for 24 hrs. For ELISA- based quantification, genomic DNA was extracted
16 (Wizard^R Genomic DNA Purification kit; Promega) and 5hmC levels were measured using
17 MethylFlashTM Global DNA Hydroxymethylation (5hmC) ELISA Easy Kit (Epigentek) and
18 normalized to DNA content, following the manufacturer instructions.

19 For immunofluorescence, cells were fixed (4% PFA) and permeabilized (0.4% Triton X-100;
20 15min at RT). After a denaturation step (2N HCl, 15min at RT) and a neutralization step (100
21 mM Tris-HCl pH 8.5, 10min at RT), cells were incubated with 0.1% Triton X-100/5% BSA for 1
22 hr. Anti 5-hmC monoclonal Antibody was incubated overnight at 4°C (1:200, HMC/4D9 A1018,
23 Epigentek) followed by anti-mouse 594 secondary antibody (Alexa Fluor Molecular Probes).

1 Images were obtained using the DM6000B microscope equipped with DFC 350FX B/W digital
2 camera (Leica Microsystems). The AF6000 (Leica Microsystems) software was used for image
3 acquisition/elaboration.

4

5 **DNA methylation data analysis**

6 DNA methylation comparison between L-Pro treated- and *Tet* TKO mESCs was performed as
7 described (17). Briefly, the *Tet* TKO hyper-DMRs (18) in which at least 3 CpGs were covered by
8 L-Pro RRBS experiments (6) were selected for the analysis. For each region, the ratio between
9 the number of hypermethylated CpGs ($\Delta_{(L-Pro vs VitC)} \geq 20\%$) and total CpGs was calculated. DMRs
10 with a ratio greater than 0.3 were defined hypermethylated. The statistical significance of
11 enrichment was determined using the one tail hypergeometric test available in R.

12

13 **Time-Lapse**

14 Images from ESCs \pm L-Pro (500 μ M) \pm esMTi and A459 tumor spheroids \pm Budesonide were
15 captured (20x) at the indicated time point, every 5 min for about 24 hrs on a Leica DMI6000B
16 equipped with a microscope incubator (Okolab).

17

18 **2D migration assays**

19 Boyden chamber assay was performed using polycarbonate transwells (8 μ m pore, Costar).
20 Briefly, A549 cells pre-treated \pm Budesonide or DMSO in complete medium. After 24 hrs, cells
21 were dissociated by trypsin-EDTA, seeded (4×10^5 cells/per insert) in DMEM/1% FBS \pm
22 Budesonide and allowed to migrate towards FBS gradient (1%-15%) for 6 hrs. Nuclei were
23 stained and migrated cells were counted (4 random fields/insert, 10x).

1 For A549 tumor spheroid assay, 2.5×10^3 FACS sorted cells were plated/well in V-shaped low
2 attachment 96-multiwell (Corning Costar) and allowed to aggregate for 4 days. Spheroids were
3 plated on gelatin-coated wells in complete medium without growth factors. After 48 hrs, tumor
4 spheroids were fixed and stained (PBS1x/6% glutaraldehyde/0.15% crystal violet) for 30min at
5 RT. The percentage of spreading spheroids was determined by quantifying the number of
6 spheroids with a crown of mesenchymal/migrating cells over the total number of spheroids
7 plated.

8

9 **3D Organotypic culture**

10 For the analysis of SUM-159-derived spheroids invasive outgrowth, single SUM-159 cells were
11 plated in 8-well chamber slides (IBIDI) onto a base layer of Matrigel and collagen I (5 mg/ml
12 and 2.3 mg/ml, respectively; BD) and supplemented with a 2% Matrigel/growth medium
13 mixture. Cultures were grown for 6 days. Medium was replenished every 2 days. SUM-159
14 spheroids were imaged for development of invasive outgrowths by differential interference
15 contrast (DIC) imaging using a 20X objective lens. Colonies circularity and area parameters
16 were calculated using ImageJ software.

17

18 **Xenograft experiments**

19 All animal experiments were approved by the OPBA (Organisms for the well-being of the
20 animal) of IFOM and Cogentech. All experiments complied with national guidelines and
21 legislation for animal experimentation. All mice were bred and maintained under specific
22 pathogen-free conditions in our animal facilities at Cogentech Consortium at the FIRC Institute
23 of Molecular Oncology Foundation and at the European Institute of Oncology in Milan, under

1 the authorization from the Italian Ministry of Health (Autorizzazione N° 604-2016). SUM-159
2 cells, expressing pLenti CMV-Puro-LUC construct (Plasmid #17477, ADDGENE), were trypsin
3 detached, washed twice, and resuspended in PBS to a final concentration of 2.5×10^6 cells/13 μ l.
4 The cell suspension was then mixed with 5 μ l growth factor–reduced Matrigel (BD) and 2 μ l
5 Trypan blue solution and maintained on ice until injection. Aseptic conditions under a laminar
6 flow hood were used throughout the surgical procedure. Female NOD.Cg-
7 Prkdcscid1l2rgtm1Wjl/SzJ (commonly known as the NOD SCID gamma; NSG) mice (6–9 week
8 old) were anesthetized with 375 mg/Kg Avertin, laid on their backs, and injected with a 20 μ l
9 cell suspension directly in the fourth mammary fad pad. After 4 days, mice were administered by
10 intraperitoneal injection (I.P.) either Budesonide (3 mg/Kg) or the same volume of carrier as
11 control, every day for 3 consecutive weeks. For bioluminescence imaging, 100 μ l of D-Luciferin
12 (30 mg/ml, Perkin Elmer) was injected I.P. before placing mice under 2% inhaled isofluorane
13 anesthesia. Bioluminescence signal was monitored every 5 days by measuring photon flux (15
14 min from I.P. injection) using IVIS LUMINA III imaging System (Perkin Elmer). Data were
15 analyzed using average counts in the ROIs and normalized to acquisition time. At the endpoint,
16 mice were sacrificed and tumors were harvested. Tumor volume was measured with digital
17 caliper and calculated according to the formula: $L \times W^2/2 = \text{mm}^3$. For histological analysis,
18 primary tumors and lung metastases were fixed in 4% phosphate-buffered formalin and paraffin-
19 embedded. The Scan Scope XT device and the Aperio Digital pathology system software
20 (Aperio) were used to collect pictures and detect metastases.

21

22 |

1 **Immunohistochemistry**

2 Formalin-fixed, paraffin-embedded (FFPE) mouse tumor tissue and lungs sections (3 μ m) were
3 incubated with 3% H₂O₂ for 5 min and then blocked with 2% goat serum in PBS for 1 hr.
4 Samples were incubated with primary antibodies (listed in Table S2) for 2 hrs at RT in 2% goat
5 serum. HRP-conjugated secondary antibodies were used and signals were developed with DAB.
6 Samples were counterstained with hematoxylin (Merck) or stained with Picrosirius Red
7 (Polysciences Inc.). Cell circularity (stained with anti Vimentin) and collagen fiber distribution
8 (observed in polarized light microscopy images) parameters were calculated using ImageJ
9 software.

10

11 **Bioinformatic analysis of PH4A2 in cancer cohorts**

12 Survival analysis was performed exploiting the METABRIC breast cancer dataset (19),
13 downloaded from the TCGA database. Expression data were extracted from the dataset (1980
14 Breast Cancer samples) and three Illumina probesets were available for P4HA2;
15 ILMN_1795778, ILMN_2381697, ILMN_2280135. mRNA expression data from the three
16 probesets for each sample were averaged and samples were grouped into Low and High P4HA2
17 expression based on the mRNA levels with respect to the mean. Data analysis was performed
18 using JMP 10.0 statistical software (SAS Institute, Inc);

19

20 **Statistical analysis**

21 Statistical significance was determined by a two-tailed paired Student's *t*-test. *p*-values ≤ 0.05
22 were considered as statistically significant. Error bars represent SEM or SD as indicated.

23

1 Results

2 High-throughput screen identifies inhibitors of embryonic stem to mesenchymal-like 3 transition (esMT)

4 We exploited the highly dynamic embryonic stem to mesenchymal-like transition (esMT) as a
5 molecular and functional paradigm for reversible cell state transition (20, 21). To search for
6 compounds able to block esMT we developed a fully automated unbiased high-throughput
7 screening (HTS) in a 96-well format based on a robust cell colony phenotype assay (CFA) (**Fig.**
8 **1A and B**). The CFA was optimized to achieve a high colony forming efficiency (72±9
9 colonies/well) and high efficiency of domed-to-flat transition (**Fig. 1A**) after L-Pro
10 supplementation (85±7% flat *vs* 12±6% domed colonies) (**Fig. 1C**; Supplementary Fig. S1A).
11 The feasibility of the assay was verified using two potent esMT antagonists, *i.e.* L-Ascorbic acid
12 (Vitamin C, VitC) and the GSK3 inhibitor CHIR99021 (16, 20), which robustly reduced the
13 fraction of flat-shaped colonies to Control levels (~90% domed *vs* ~10% flat colonies) (**Fig. 1C**;
14 Supplementary Fig. S1A). We employed this automated CFA to screen a Prestwick chemical
15 library® containing 1,200 FDA-approved small molecules. ESCs were plated in the presence of
16 L-Pro and exposed to either drugs or solvent (DMSO). At day four after plating, colonies were
17 fixed and stained with a glutaraldehyde/crystal violet mix and subjected to phenotypic analysis
18 (**Fig. 1D**). A substantial number of the drugs uniformly distributed throughout the plates (137,
19 11.4%) completely inhibited cell colony formation (Table S3). In depth analysis of these ESC
20 inhibitors (ESCi) revealed that: i) the large majority (80%) have anticancer activities (Table S4);
21 ii) ~50% belongs to 5 therapeutic classes of the 135 covered by the library (**Fig. 1E and F**); and
22 iii) their activities rely on specific structural constraints (**Fig. 1G**; Supplementary Fig. S1B and
23 S1C). We next restricted the analysis to the drugs able to inhibit esMT, *i.e.* to significantly

1 reduce the fraction of L-Pro-induced atypical/flat colonies and increase the fraction of
2 round/domed-shaped colonies. Fourteen esMT inhibitors [(esMTi) 1.2%; Table S5] were
3 selected and validated in secondary CFAs (**Fig. 1H**; Supplementary Fig. S1D). Consistent with
4 their antagonistic effect on esMT, the three most active drugs, Budesonide, Spiramycin and
5 Propafenone (Supplementary Fig. S1E) prevented cell motility and induction of esMT markers
6 (**Fig. 2A**; Supplementary Fig. S2A). Notably, Budesonide, Spiramycin and Propafenone
7 prevented neither L-Pro induced down-regulation of Aminoacid stress response (AAR) pathway
8 markers (**Fig. 2B**) nor cell proliferation (**Fig. 2C**), which are the earliest ESC responses to L-Pro
9 supplementation and depend on L-Pro -tRNA loading (21). Finally, we tested their ability to
10 promote the reversal mesenchymal-like-to-embryonic-stem-cell transition [MesT; (20)]. To this
11 end, L-Pro-induced mesenchymal-like cells (PiCs) were plated at low density and treated with L-
12 Pro \pm esMTi or VitC as control (**Fig. 2D**). Cells reverted back to the ESC phenotype in the
13 presence of esMTi, with efficiency comparable to that observed for VitC (**Fig. 2D**). These results
14 indicate that esMTi specifically block esMT acting downstream of L-Pro -tRNA loading, and
15 induce MesT even in a highly rich L-Pro environment.

16

17 **Collagen accumulation underpins esMT**

18 To obtain mechanistic insights into esMT, we classified the 14 esMTi identified in the screening
19 on the basis of their chemical properties. Despite belonging to 9 different classes (Tanimoto
20 coefficient $T > 0.75$) (Supplementary Fig. S2B), nearly 50% of the esMTi, including Budesonide,
21 are inhibitors of collagen accumulation/fibrosis *in vitro* and/or *in vivo* (Table S6), pointing to a
22 link between collagen accumulation and esMT. Notably, we recently showed that L-Pro -induced
23 esMT depends on protein synthesis and that ESCs are specifically and intrinsically starved of L-

1 Pro (21). Based on our findings and these considerations, and given that L-Pro and 4-*trans*-
2 hydroxyproline (HyP) are the major components of collagen, we hypothesized that L-Pro
3 supplementation would increase collagen synthesis/hydroxylation in ESCs, eventually inducing
4 esMT. Accordingly, Collagen (Coll1a1) and collagen hydroxyproline (C-Hyp) levels both
5 increased in L-Pro treated ESCs, accumulating primarily in the endoplasmic reticulum (ER; **Fig.**
6 **2 E and F**; Supplementary Fig. S2C). Conversely, the esMTi Budesonide prevented *Coll1a1*
7 expression at RNA and protein levels, as well as C-Hyp in L-Pro-treated cells (**Fig 2G-J**;
8 Supplementary Fig. S2D). Budesonide is a 21-hydroxysteroid glucocorticoid; however, none of
9 the other twenty-four 21-hydroxysteroids derivatives, including the glucocorticoid
10 Dexamethasone, was identified as a positive hit in the primary screening (Supplementary Fig.
11 S2E) and confirmed in the secondary CFA (Supplementary Fig. S2F), thus revealing a highly
12 specific effect of Budesonide. Of note, among the 25 21-hydroxysteroids included in the library,
13 only Budesonide is classified as a high-affinity Glucocorticoid Receptor (GR) antagonist in
14 different databases, including [Pubchem
15 (<https://pubchem.ncbi.nlm.nih.gov/compound/5281004>), DrugBank
16 (<https://www.drugbank.ca/drugs/DB01222>) and Therapeutic Target Database
17 (<https://db.idrblab.org/ttd/drug/d0y7iu>). This raised the possibility that Budesonide specificity
18 might be due, at least in part, to its activity as GR antagonist. Interestingly, addition of another
19 established antagonist of GR, Mifepristone, was able to block esMT similarly to Budesonide
20 (Supplementary Fig. S2F). Furthermore, Budesonide but not Dexamethasone reduced the levels
21 of the well known GR target Alkaline Phosphatase (22), while keeping ESC undifferentiated
22 (Supplementary Fig. S2G). Finally, Budesonide fully counteracted Dexamethasone- induced
23 overexpression of the GR target genes *Fkbp5* and *Tfcp2l1* (Supplementary Fig. S2H).

1 Glucocorticoids, including Dexamethasone, are commonly used to induce collagens in cultured
2 cells. Of note, we found that Budesonide but not Dexamethasone fully counteracted L-Pro -
3 dependent increase of Col1a and C-HyP (**Fig. 2G-J**; Supplementary Figure S2I).

4 Together these findings supported the hypothesis that L-Pro -induced esMT depends on L-Pro -
5 mediated induction of collagen synthesis/hydroxylation, and indicated that Budesonide
6 counteracts this effect (**Fig. 2K**).

7

8 **Genetic and pharmacological inhibition of collagen hydroxylation prevents esMT**

9 To directly test our hypothesis, and given that it is not feasible to knock-out all the members of
10 the collagen family, we decided to interfere with collagen hydroxylation by targeting the Prolyl-
11 4-hydroxylases (P4Hs). P4H enzymes belong to the family of VitC/Fe⁺²/αKG-dependent
12 dioxygenases, and form tetrameric (α₂:β₂) complexes able to catalyze the hydroxylation of L-Pro
13 residues in nascent collagens in the ER. Two out of the three genes coding for the alpha subunit
14 of P4H, *i.e.* *P4ha1* and 2, were expressed at similar levels in ESCs, whereas *P4ha3* expression
15 was nearly undetectable (Supplementary Fig. S3A). Of note, *P4HA2* has been recently associated
16 with collagen production and tumor progression of human breast cancer (23). We thus
17 inactivated *P4ha2* in ESCs by CRISPR/Cas9 and selected two independent clones (*P4ha2*^{KO} #1
18 and #2) that carry different genomic deletions at the boundary between exon 6 and intron 7,
19 leading to a frame-shift and the formation of a premature stop codon (**Fig. 3A**; Supplementary
20 Fig. S3B). Both *P4ha2*^{KO} ESCs preserved the typical domed morphology, were highly AP
21 positive (**Fig. 3B**), and retained the expression of key pluripotency markers (Supplementary Fig.
22 S3C and S3D). To avoid the possibility that *P4ha1* may, at least partially, compensate for the
23 lack of *P4ha2* we knocked down *P4ha1* in *P4ha2*^{KO} ESCs using two shRNAs, which target non-

1 overlapping *P4ha1* mRNA sequences (**Fig. 3C**; Supplementary Fig. S3E). *P4ha2^{KO}/P4ha1^{KD}*
2 ESCs retained AP activity and expression of pluripotency genes (**Fig. 3B**; Supplementary Fig.
3 S3C and S3D). We then examined the effect of *P4ha2^{KO}* and *P4ha2^{KO}/P4ha1^{KD}* on L-Pro-
4 induced esMT. Control ESCs (NT) retained high frequency of atypical colonies in response to L-
5 Pro, while *P4ha2^{KO}* ESCs mostly developed typical domed colonies lacking the crown of
6 mesenchymal-like cells scattered around the colony core (**Fig. 3D**). Remarkably, this phenotype
7 was robustly enhanced in two independent *P4ha2^{KO}/P4ha1^{KD}* clones (**Fig. 3D**), indicating that
8 *P4ha1* partially compensates the lack of *P4ha2*. Consistent with the inhibitory effect on L-Pro-
9 induced phenotypic transition (domed-flat), cell motility was also impaired in P4H deficient
10 ESCs (Supplementary Fig. S3F). Conversely, L-Pro-induced proliferation (**Fig. 3E**) or alleviation
11 of AAR pathway (Supplementary Fig. S3G) was preserved, providing evidence that P4H activity
12 is specifically required for L-Pro- induced esMT. Finally, as expected, C-Hyp accumulation was
13 strongly reduced in P4H deficient ESCs (**Fig. 3F**). Together, these findings indicate that *P4ha*
14 genetic ablation prevents collagen hydroxylation and antagonizes esMT mimicking the
15 phenotypic and molecular effects of Budesonide, thus supporting the concept that esMT is
16 functionally linked to collagen hydroxylation.

17

18 **Inhibition of collagen hydroxylation enhances VitC-dependent DNA and histone** 19 **hydroxylation/demethylation in pluripotent stem cells**

20 Collagen hydroxylation requires VitC and our findings indicate that this crucial post-translational
21 modification of collagen underpins L-Pro -induced esMT. However, exogenously added VitC
22 antagonizes rather than induces esMT (Comes et al., 2013; **Fig. 1C**; Supplementary Fig. S1A)
23 without blocking C-HyP accumulation (**Fig. 2I and J**). This apparent contradiction could be

1 reconciled by assuming the existence of a VitC-dependent mechanism that overcomes the
2 agonistic effect of collagen hydroxylation on esMT (**Fig. 2K**). Of note, besides P4H, VitC is
3 essential for the activity of different enzymes belonging to the family of $\text{Fe}^{+2}/\alpha\text{KG}$ -dependent
4 dioxygenases with different substrate specificity, including DNA (TET) and Histones (JMJ),
5 subcellular localization (cytoplasm, ER and nucleus), expression levels and kinetics parameters.
6 Hence, we hypothesized that a sudden increase of collagen hydroxylation might channel VitC to
7 the ER for the activity of collagen hydroxylases (P4Hs), concomitantly provoking its
8 stoichiometric reduction in other cellular compartment, which translates into reduced activity of
9 VitC-dependent dioxygenases, ultimately inducing esMT. Of note, we expect that such a
10 substantial perturbation of VitC homeostasis might occur only in a VitC-limiting environment
11 when collagen synthesis is induced.

12 To test our hypothesis we asked whether a compartmentalized VitC-dependent reaction, i.e
13 collagen hydroxylation in the ER, might impact on the activity of VitC/ $\text{Fe}^{+2}/\alpha\text{KG}$ -dependent
14 TET and JMJ dioxygenases and thus on DNA and histone methylation levels. We first compared
15 the DNA methylation profiles of L-Pro- treated ESCs (6) and the *Tet* triple KO (TKO) ESCs (18)
16 and found that 54% of the TET target regions were hypermethylated in L-Pro-treated cells at
17 early time point (day 2), which increased up to 89% at day 5 (**Fig. 3G**). Prompted by these
18 results, we evaluated the impact of *P4h* KO on the global levels of DNA hydroxymethylation
19 (5hmC), which depends on the activity of TET enzymes. In a high-L-Pro/low-VitC condition,
20 5hmC levels rapidly decreased in control but not in P4Hs deficient ESCs (**Fig. 3 H and I**;
21 Supplementary Fig. S3H). Similarly, Budesonide counteracted the reduction of 5hmC in wild-
22 type ESCs (Supplementary Fig. S3I). We then evaluated the impact of *P4h* KO on JMJ
23 dioxygenases, which target removal of H3K9/36 methylation and assessed whether VitC

1 supplementation blunted the effect of L-Pro. In a high-L-Pro/low-VitC environment the global
2 levels of both H3K9me3 and H3K36me3 increased in Control but not in *P4ha2^{KO}* and
3 *P4ha2^{KO}/P4ha1^{KD}* ESCs (**Fig. 3J**; Supplementary Fig. S3J). Notably, H3K9me3 levels were
4 even lower in the *P4ha2^{KO}/P4ha1^{KD}* double mutant compared to *P4ha2^{KO}* (**Fig. 3J**), consistent
5 with the idea that VitC availability may progressively increase in the nucleus as C-Hyp levels
6 decrease in the ER (**Fig. 3F**). In keeping with the idea that VitC is a limiting metabolite in ESCs
7 (12), its addition not only prevented L-Pro- dependent increase of H3K9me3 levels but also
8 further reduced H3K9me3 global levels in a low L-Pro environment (**Fig. 3K**). Furthermore,
9 Budesonide mimicked the antagonistic effect of VitC, preventing both L-Pro -dependent esMT
10 (**Fig. 1 C and H**; **Fig. 2A**; Supplementary Fig. S1A) and increase of H3K9me3 levels
11 (Supplementary Fig. S3K). Of note, neither L-Pro, nor Budesonide modified the expression of the
12 specific DNA/histone demethylases, including *Tet1*, *2*, *3* and *Jmjd2c* (H3K9me2/me3 and
13 H3K36me2/me3 demethylation; Supplementary Fig. S3L) ruling out the possibility the observed
14 epigenetic changes reflects altered expression of the enzymes.

15 Collectively, these findings indicate that increased collagen hydroxylation causes DNA and
16 histones methylation, and suggest that this occurs by altering VitC homeostasis and reducing the
17 activity of nuclear dioxygenases (**Fig. 3L**). Budesonide and P4H deficiency interferes with this
18 metabolic perturbation by reducing collagen hydroxylation with different mechanisms.
19 Specifically, Budesonide blocks collagen synthesis at RNA and protein levels, and as a
20 consequence reduces collagen hydroxylation; whereas, P4H deficiency directly interferes with
21 hydroxylation of nascent collagens within the ER.

22 **Collagen hydroxylation influences the epigenetic landscape of tumor cells and induces cell**
23 **state transition**

1 The above results raise the possibility that this mechanism might be general applicable to
2 mesenchymal transition processes and critically important in pathological situations, such as
3 cancer progression and metastatic dissemination. Consistent with the inhibitory effects on L-Pro -
4 induced esMT in ESCs, Budesonide robustly inhibited human lung cancer A549 cell migration *in*
5 *vitro*, in tumor spheroid and Boyden chambers assays (**Fig. 4 A and B**; Supplementary Fig. S4A-
6 C), without affecting cell proliferation (Supplementary Fig. S4D). Furthermore, similar to what
7 observed in pluripotent stem cells, Budesonide reduced collagen accumulation in A549 at RNA
8 and protein level (**Fig. 4C**; Supplementary Fig. S4E). We thus went on and assessed the effect of
9 Budesonide on histone methylation, by analyzing the global levels of different methylation
10 marks including H3K9me2/me3, H3K36me3, H3K27me3 and H3K4me3, which are the known
11 substrates of the dioxygenases involved in histone demethylation. Remarkably, Budesonide
12 significantly reduced global histone methylation in A549 cells (**Fig. 4D**) suggesting that an
13 antagonistic interplay between collagen and histone hydroxylation occurs in cancer cells. To get
14 further mechanistic insights into this phenomenon, we knocked down *P4HA2* in A549
15 (Supplementary Fig. S4F-G) and confirmed that C-Hyp accumulation was strongly reduced
16 compared to NT control cells (**Fig. 4E**). Consistent with what observed in ESCs, *P4HA2^{KD}*
17 strongly reduced A549 cell migration (**Fig. 4F**; Supplementary Fig. S4H) but not proliferation
18 (Supplementary Fig. S4I), and significantly reduced histone methylation (**Fig. 4G**).

19 Prompted by these results and to validate the model in a different tumor type, we focused on
20 breast cancer. Interestingly, elevated expression of P4HA2 has been recently associated with
21 poor prognosis in a variety of breast cancers (24). We first extended and corroborated the latter
22 observations by analyzing P4HA2 expression levels in an independent Breast Cancer dataset,
23 encompassing nearly 2000 patients with complete clinical-pathological follow up. We found that

1 elevated level of P4HA2 is significantly associated with decrease survival, and, more relevantly,
2 is an independent predictor of disease outcome with respect to a set of standard
3 clinicopathological parameters in multivariate analysis (**Fig. 5A**).

4 To further explore this mechanism, we investigated the effect of *P4HA2^{KD}* on the triple negative
5 breast cancer (TNBC) cell line SUM159, which are characterized by a high degree of
6 heterogeneity/plasticity and recapitulates the key features of collective invasion typical of human
7 breast cancers (25). Interestingly, we found that interfering with *P4HA2* expression (**Fig. 5B**)
8 converted SUM159 cells to a more epithelial-like state (**Fig. 5 C and D**), without affecting cell
9 proliferation (**Fig. 5E**), and reduces C-Hyp levels (**Fig. 5F**). Of note, *P4HA2^{KD}* reduced the
10 global levels of different methylation marks including H3K27me3, H3K36me3, H3K4me3,
11 H3K9me2/me3 and (**Fig. 5G**). To investigate this phenotype further, we assessed the effect of
12 Budesonide and first confirmed that it reduced Colla1 and C-Hyp accumulation in SUM159
13 cells (**Fig. 6 A and B**). Remarkably, Budesonide treatment concomitantly led to reduction of
14 H3K9me2/3, H3K36me3 and H3K27me3 but not H3K4me3 levels (**Fig. 6C**). Of note,
15 expression of the specific dioxygenases involved in histone demethylation, including *JMJD3*
16 (H3K27me3), *JMJD2A* (H3K9me2/me3 and H3K36me2/me3) and *JARID1A* (H3K4me3) was
17 not affected (Supplementary Fig. S5A), thus further supporting the idea that the global reduction
18 of histone methylation was due to increased activity rather than expression of these enzymes.

19 Complementary to these findings, we showed that VitC supplementation significantly reduced
20 H3K9me2/3, H3K27me3 and H3K4me3 in a dose- and histone mark- dependent manner (**Fig.**
21 **6D**), indicating that VitC is a limiting factor for proper function of JMJ demethylases in
22 SUM159 cells, and further supporting the idea that variations in the levels and/or
23 compartmentalization of VitC impacts on the activity of nuclear dioxygenases in cancer cells.

1 All together these findings indicate that collagen synthesis/hydroxylation underpins cell state
2 transition dynamics, and influences the epigenetic status of normal and tumor cells.

3

4 **Budesonide blocks metastatic dissemination of TNBC cells by preventing collagen** 5 **deposition and mesenchymal transition**

6 Prompted by these results and the potential therapeutic relevance of targeting mesenchymal
7 transition as a strategy to prevent tumor cell dissemination, we further investigated the effect of
8 Budesonide on SUM159 cells. First, we tested the impact of Budesonide on SUM159 cell
9 invasion using a 3D organotypic culture (**Fig. 7A**). Treatment with Budesonide robustly reduced
10 the collective invasive ability of SUM159 spheroids and significantly increased colony
11 compaction and circularity in a dose dependent fashion (**Fig. 7B**; Supplementary Fig. S5B),
12 without affecting cell proliferation (Supplementary Fig. S5C). We further corroborated these *in*
13 *vitro* findings using an experimental metastatic murine model. To this end, we orthotopically
14 injected luciferase-expressing SUM159 cells into the mammary fat pad of immunocompromised
15 mice. Budesonide treatment altered significantly the cell shape and stromal collagenolytic
16 organization of primary tumors, which were composed of cuboidal, epithelioid cells with a
17 reduced and less organized collagen-surrounding matrix (**Fig. 7C and D**). On the contrary, in
18 control animal primary tumors were primarily composed of elongated, spindle shaped cells
19 surrounded by a thick collagenous stromal desmoplastic reaction (**Fig. 7C and D**). Consistently,
20 Budesonide treatment reduced primary tumors volume (Supplementary Fig. S5D and E), but had
21 no effect on the number of KI67 and Caspase positive cells (Supplementary Fig. S5F).
22 Remarkably, instead, it completely abrogated the development of metastatic foci into the lung
23 (**Fig. 7 E and F**). Collectively, these findings indicate that Budesonide-mediated interference

- 1 with collagen production/deposition hampers mesenchymal transition state, ultimately impairing
- 2 metastatic dissemination.
- 3

1 **Discussion**

2 Collagen hydroxylation and DNA/histone hydroxylation/demethylation are catalyzed by
3 dioxygenases superfamily enzymes, namely the prolyl 4-hydroxylases (P4Hs) in the endoplasmic
4 reticulum (ER), and Ten-Eleven Translocation (TET) and Jumonji (JMJ) demethylases in the
5 nucleus, respectively. Here, we demonstrate that collagen and DNA/histone hydroxylation show
6 an antagonistic interplay. Mechanistically, we propose that this previously unexplored interplay
7 relies on the availability VitC, which is an essential cofactor for the activity of both P4Hs and
8 TET/JMJ. This idea is in line with emerging evidence that reduced availability of dioxygenases
9 substrates/cofactors, such as O₂ and VitC, promotes cell state transition and metastatic
10 dissemination by reducing the activity of TET and JMJ demethylases with a concomitant
11 increase of DNA and histone methylation (26, 27). Here we propose that collagen prolyl
12 hydroxylation is a previously unexplored key component of this mechanism. Several lines of
13 evidence support our model. First, genome wide analyses in embryonic stem cells (ESCs) reveal
14 that a large fraction of TET1-3 target DNA regions are methylated after exposure to a high L-Pro
15 regimen, which results in increased collagen synthesis/hydroxylation. Second, increased collagen
16 synthesis/hydroxylation under VitC limiting conditions rapidly reduces 5hmC and increases
17 H3K9/K36 histone methylation, which is in agreement with a reduced activity of TET and JMJ,
18 respectively. Finally, interfering with collagen synthesis/hydroxylation, by either
19 pharmacological treatment with the glucocorticoid Budesonide (collagen synthesis) or genetic
20 ablation of P4HA2 (collagen hydroxylation), blocks cell state transition in pluripotent stem cells
21 and tumor cells.

22 Of note, the latter findings are highly relevant for cancer biology as high P4HA2 expression is a
23 poor prognostic marker in breast cancer patients and correlates with the metastatic progression of

1 triple negative breast cancer (TNBC) cells (24) and our findings). Accordingly, we demonstrate
2 that P4HA2 knockdown reduces global H3K9, H3K36, H3K4 and H3K27 methylation levels and
3 reverts the mesenchymal phenotype of TNBC SUM159 cells to a more epithelial-like phenotype.
4 Of note, the TNBC SUM159 cells are highly heterogeneous and can be sorted into low and high
5 tumor-initiating populations based on the expression of the basal epithelial marker integrin- β 4
6 (ITGB) (28). Interestingly, we noticed that P4HA2 expression is significantly higher in the fully
7 mesenchymal ITGB^{low} subpopulation vs the ITGB^{high} subpopulation that show hybrid
8 epithelial/mesenchymal phenotype (28). Although further studies are necessary, we speculate
9 that this collagen hydroxylation/P4HA2 -dependent remodeling of the epigenetic landscape may
10 underlie, at least in part, the molecular and functional heterogeneity of TNBC cells.

11 In line with our idea, pharmacological targeting of this collagen-epigenetic axis with
12 Budesonide, identified in this study, inhibits the metastatic dissemination of SUM159 cells by
13 preventing mesenchymal-transition. Interestingly, Budesonide, has been very recently identified
14 in a combined connectivity mapping and pharmacoepidemiological approach as a drug with
15 potential breast cancer-preventing properties (29). Moreover, Budesonide is universally
16 employed to treat asthma, and asthma was recently associated with reduced risk of developing
17 pancreatic ductal adenocarcinoma (PDAC) (30). Furthermore, Budesonide is also used to treat
18 the collagenous colitis, a rare inflammatory disorder associated with collagen accumulation in
19 the colorectal mucosa (31, 32), and its therapeutic efficacy is ascribed to the anti-inflammatory
20 activity of GCs (33). Thus, our unexpected findings that Budesonide blocks mesenchymal
21 transition interfering with collagen accumulation provide novel insights into its therapeutic
22 effects. Of note, the mechanism behind the effects of Budesonide remains to be fully clarified.
23 Indeed, although our findings raised the possibility of potential involvement of the GR, the

1 mechanism may prove more complex and its complete elucidation will require further
2 investigations. Specifically, we cannot rule out the possibility that off-target effects of
3 Budesonide at the concentration used, including for instance inhibition of P4H activity, could be
4 responsible of the observed phenotypes.

5 Epigenetic mechanisms may govern the accumulation of collagen by reducing promoter
6 methylation and increasing expression of collagen genes (34, 35). Disruption of this epigenetic-
7 >collagen axis is considered as the main cause of the deregulation of collagen deposition during
8 aging and in pathological conditions, including tumorigenesis (36). Here we reveal the existence
9 of a reverse collagen->epigenetic functional axis associated with cell state transition in normal
10 and pathological conditions.

11 In conclusion, our findings provide evidence of a previously unexplored functional interplay
12 between collagen and DNA/Histone hydroxylation and identify P4HA2 as a key component of
13 this mechanism. Interestingly, it has been recently reported that expression of another member of
14 P4H family, P4ha1, reduces prolyl-hydroxylation of HIF-1 α by modulating the levels of
15 ketoglutarate (KG) and succinate in the cytoplasm (37). Of note, hydroxylation of HIF-1 α is
16 catalyzed by the Prolyl hydroxylases (PHDs), which are VitC-dependent dioxygenase belonging
17 to the same family of TET and JMJ. The evidences from this paper of a collagen hydroxylation
18 (ER) -> HIF hydroxylation (cytoplasm) axis strongly support our findings and can be well
19 explained with the model proposed herein.

20 Finally, we identify Budesonide as a potent inhibitor of this mechanism and a novel drug
21 candidate for the treatment of a broad spectrum of diseases in which cell fate transition and
22 fibrosis are involved, including metastatic cancer.

23

1 **Acknowledgments**

2 We are grateful to members of the Integrated Microscopy and FACS Facilities of IGB-ABT,
3 CNR, and to Gabriele Di Napoli for excellent technical assistance. We are indebted to Stefano
4 Confalonieri at European Institute of Oncology, Milan, for the bioinformatic analysis of PH4A2
5 in cancer cohorts. We are most grateful to Prof. Francisco X. Real for discussion and helpful
6 suggestions. This study was supported by AIRC (IG 20736), MIUR Epigenomics Flagship
7 Project (EPIGEN) and POR Campania FESR 2014/2020 (Project SATIN) to G.M.

8

9

10

11

1 **References:**

- 2 1. Chaffer CL, San Juan BP, Lim E, Weinberg RA. EMT, cell plasticity and metastasis.
3 *Cancer Metastasis Rev.* 2016;35:645-54.
- 4 2. Nieto MA, Huang RY, Jackson RA, Thiery JP. Emt: 2016. *Cell.* 2016;166:21-45.
- 5 3. Varga J, Greten FR. Cell plasticity in epithelial homeostasis and tumorigenesis. *Nat Cell*
6 *Biol.* 2017;19:1133-41.
- 7 4. Valastyan S, Weinberg RA. Tumor metastasis: molecular insights and evolving
8 paradigms. *Cell.* 2011;147:275-92.
- 9 5. Reid MA, Dai Z, Locasale JW. The impact of cellular metabolism on chromatin
10 dynamics and epigenetics. *Nat Cell Biol.* 2017;19:1298-306.
- 11 6. D'Aniello C, Cermola F, Patriarca EJ, Minchiotti G. Vitamin C in Stem Cell Biology:
12 Impact on Extracellular Matrix Homeostasis and Epigenetics. *Stem Cells Int.*
13 2017;2017:8936156.
- 14 7. Esteban MA, Pei D. Vitamin C improves the quality of somatic cell reprogramming.
15 *Nature genetics.* 2012;44:366-7.
- 16 8. Chen J, Guo L, Zhang L, Wu H, Yang J, Liu H, et al. Vitamin C modulates TET1
17 function during somatic cell reprogramming. *Nature genetics.* 2013;45:1504-9.
- 18 9. Wang T, Chen K, Zeng X, Yang J, Wu Y, Shi X, et al. The histone demethylases
19 Jhdm1a/1b enhance somatic cell reprogramming in a vitamin-C-dependent manner. *Cell Stem*
20 *Cell.* 2011;9:575-87.
- 21 10. Hore TA, von Meyenn F, Ravichandran M, Bachman M, Ficz G, Oxley D, et al. Retinol
22 and ascorbate drive erasure of epigenetic memory and enhance reprogramming to naive
23 pluripotency by complementary mechanisms. *Proc Natl Acad Sci U S A.* 2016;113:12202-7.
- 24 11. Blaschke K, Ebata KT, Karimi MM, Zepeda-Martinez JA, Goyal P, Mahapatra S, et al.
25 Vitamin C induces Tet-dependent DNA demethylation and a blastocyst-like state in ES cells.
26 *Nature.* 2013.
- 27 12. D'Aniello C, Habibi E, Cermola F, Paris D, Russo F, Fiorenzano A, et al. Vitamin C and
28 l-Proline Antagonistic Effects Capture Alternative States in the Pluripotency Continuum. *Stem*
29 *Cell Reports.* 2017;8:1-10.
- 30 13. Agathocleous M, Meacham CE, Burgess RJ, Piskounova E, Zhao Z, Crane GM, et al.
31 Ascorbate regulates haematopoietic stem cell function and leukaemogenesis. *Nature.*
32 2017;549:476-81.
- 33 14. Cimmino L, Dolgalev I, Wang Y, Yoshimi A, Martin GH, Wang J, et al. Restoration of
34 TET2 Function Blocks Aberrant Self-Renewal and Leukemia Progression. *Cell.* 2017;170:1079-
35 95 e20.
- 36 15. Zhao Z, Wang L, Di LJ. Compartmentation of metabolites in regulating epigenome of
37 cancer. *Mol Med.* 2016;22.
- 38 16. Casalino L, Comes S, Lambazzi G, De Stefano B, Filosa S, De Falco S, et al. Control of
39 embryonic stem cell metastability by L-proline catabolism. *J Mol Cell Biol.* 2011;3:108-22.
- 40 17. Gatto S, Gagliardi M, Franzese M, Leppert S, Papa M, Cammisa M, et al. ICF-specific
41 DNMT3B dysfunction interferes with intragenic regulation of mRNA transcription and
42 alternative splicing. *Nucleic Acids Res.* 2017;45:5739-56.
- 43 18. Lu F, Liu Y, Jiang L, Yamaguchi S, Zhang Y. Role of Tet proteins in enhancer activity
44 and telomere elongation. *Genes Dev.* 2014;28:2103-19.

- 1 19. Curtis C, Shah SP, Chin SF, Turashvili G, Rueda OM, Dunning MJ, et al. The genomic
2 and transcriptomic architecture of 2,000 breast tumours reveals novel subgroups. *Nature*.
3 2012;486:346-52.
- 4 20. Comes S, Gagliardi M, Laprano N, Fico A, Cimmino A, Palamidessi A, et al. L-Proline
5 induces a mesenchymal-like invasive program in embryonic stem cells by remodeling H3K9 and
6 H3K36 methylation. *Stem cell reports*. 2013;1:307-21.
- 7 21. D'Aniello C, Fico A, Casalino L, Guardiola O, Di Napoli G, Cermola F, et al. A novel
8 autoregulatory loop between the Gcn2-Atf4 pathway and L-Proline metabolism controls stem cell
9 identity. *Cell Death Differ*. 2015;22:1234.
- 10 22. Canalis E. Effect of glucocorticoids on type I collagen synthesis, alkaline phosphatase
11 activity, and deoxyribonucleic acid content in cultured rat calvariae. *Endocrinology*.
12 1983;112:931-9.
- 13 23. Xiong G, Deng L, Zhu J, Rychahou PG, Xu R. Prolyl-4-hydroxylase alpha subunit 2
14 promotes breast cancer progression and metastasis by regulating collagen deposition. *BMC*
15 *Cancer*. 2014;14:1.
- 16 24. Gilkes DM, Chaturvedi P, Bajpai S, Wong CC, Wei H, Pitcairn S, et al. Collagen prolyl
17 hydroxylases are essential for breast cancer metastasis. *Cancer Res*. 2013;73:3285-96.
- 18 25. Westcott JM, Precht AM, Maine EA, Dang TT, Esparza MA, Sun H, et al. An
19 epigenetically distinct breast cancer cell subpopulation promotes collective invasion. *J Clin*
20 *Invest*. 2015;125:1927-43.
- 21 26. Thienpont B, Steinbacher J, Zhao H, D'Anna F, Kuchnio A, Ploumaki A, et al. Tumour
22 hypoxia causes DNA hypermethylation by reducing TET activity. *Nature*. 2016;537:63-8.
- 23 27. Shenoy N, Bhagat T, Nieves E, Stenson M, Lawson J, Choudhary GS, et al. Upregulation
24 of TET activity with ascorbic acid induces epigenetic modulation of lymphoma cells. *Blood*
25 *Cancer J*. 2017;7:e587.
- 26 28. Bierie B, Pierce SE, Kroeger C, Stover DG, Pattabiraman DR, Thiru P, et al. Integrin-
27 beta4 identifies cancer stem cell-enriched populations of partially mesenchymal carcinoma cells.
28 *Proc Natl Acad Sci U S A*. 2017;114:E2337-E46.
- 29 29. Busby J, Murray L, Mills K, Zhang SD, Liberante F, Cardwell CR. A combined
30 connectivity mapping and pharmacoepidemiology approach to identify existing medications with
31 breast cancer causing or preventing properties. *Pharmacoepidemiol Drug Saf*. 2018;27:78-86.
- 32 30. Gomez-Rubio P, Zock JP, Rava M, Marquez M, Sharp L, Hidalgo M, et al. Reduced risk
33 of pancreatic cancer associated with asthma and nasal allergies. *Gut*. 2017;66:314-22.
- 34 31. Delarive J, Saraga E, Dorta G, Blum A. Budesonide in the treatment of collagenous
35 colitis. *Digestion*. 1998;59:364-6.
- 36 32. Tromm A, Griga T, Mollmann HW, May B, Muller KM, Fisseler-Eckhoff A. Budesonide
37 for the treatment of collagenous colitis: first results of a pilot trial. *Am J Gastroenterol*.
38 1999;94:1871-5.
- 39 33. Bonderup OK, Hansen JB, Birket-Smith L, Vestergaard V, Teglbjaerg PS, Fallingborg J.
40 Budesonide treatment of collagenous colitis: a randomised, double blind, placebo controlled trial
41 with morphometric analysis. *Gut*. 2003;52:248-51.
- 42 34. O'Reilly S. Epigenetics in fibrosis. *Mol Aspects Med*. 2017;54:89-102.
- 43 35. Zhang X, Hu M, Lyu X, Li C, Thannickal VJ, Sanders YY. DNA Methylation Regulated
44 Gene Expression in Organ Fibrosis. *Biochim Biophys Acta*. 2017.
- 45 36. Lu P, Weaver VM, Werb Z. The extracellular matrix: a dynamic niche in cancer
46 progression. *J Cell Biol*. 2012;196:395-406.

1 37. Xiong G, Stewart RL, Chen J, Gao T, Scott TL, Samayoa LM, et al. Collagen prolyl 4-
2 hydroxylase 1 is essential for HIF-1alpha stabilization and TNBC chemoresistance. Nat
3 Commun. 2018;9:4456.

4
5

1 **Figure Legends**

2 **Figure 1.** HTS-based identification of drugs that block esMT. (A) Photomicrographs of colony
3 types. (B) Miniaturization of the colony phenotype-based drug-screening method. (C) Colony
4 type quantification (domed vs flat) of ESCs treated with L-Pro (250 μ M) \pm VitC (150 μ M) or
5 CHIR99021 (CHIR, 3 μ M) or left untreated (day5). Data are mean \pm SD ($*p\leq 0.001$; ~ 100 colonies
6 scored/condition n=5). (D) Representative pictures of the screening results. Red and green circles
7 indicate ESC inhibitors (no colonies) and esMT inhibitors (domed-shaped colonies),
8 respectively. (E) Enrichment of ESC inhibitors in specific therapeutic classes (Z-score test,
9 $p<0.0001$). (F) Molecular target(s) of ESC inhibitors from PubChem/PubMed databases. (G)
10 Structure-activity relationship of drugs belonging to the Ca²⁺-channel blockers 1,4-
11 dihydropyridines. (H) Colony type quantification of ESCs treated \pm L-Pro \pm esMT inhibitors
12 (day5). DMSO was used as control. VitC and CHIR99021 were used as positive controls. Data
13 are mean \pm SD ($*p\leq 0.001$; ~ 100 colonies scored/condition n=5).

14
15 **Figure 2.** Molecular and functional characterization of esMT inhibitors. (A-C) Effect of
16 Budesonide, Spiramycin, Propafenone on L-Pro -induced cell motility (A), down-regulation of
17 AAR markers (B) and cell proliferation (C). DMSO is used as control. Representative frames of
18 time-lapse series from untreated (-L-Pro) and L-Pro \pm esMTi treated ESCs. Images were captured
19 from day 3 to 4 post plating (A). qPCR analysis of *Atf4*, *Trb3* and *Nupr1* expression. Data are
20 fold change vs untreated after normalization to *Gapdh* and are mean \pm SEM ($*p\leq 0.01$; n=3) (B).
21 FACS analysis of EdU incorporation. Data are shown as fold change vs untreated and are
22 mean \pm SEM ($*p\leq 0.01$; n=3) (C). (D) Effect of Budesonide, Spiramycin, Propafenone on the
23 reversed mesenchymal-like to embryonic stem cell transition (MesT). Freshly generated L-Pro-

1 treated ESCs (mesenchymal-like flat colonies) were plated with L-Pro \pm the indicated compounds
2 and analyzed at day 5. Colony type quantification (domed vs flat; *left*). Data are mean \pm SD
3 ($*p\leq 0.01$; ~ 100 colonies scored/condition; $n=3$). Representative pictures of L-Pro \pm esMTi or
4 VitC -treated ESCs (*middle*). Effect of L-Pro, VitC and Budesonide on esMT and MesT (*right*).
5 (E) Western blot analysis of Colla1 (*top*) and Collagen Hydroxyproline (C-HyP; *bottom*) in
6 ESCs \pm L-Pro (1mM). Densitometric analysis (ADU) is shown as fold change vs untreated ESCs.
7 Data are mean \pm SEM ($*p\leq 0.01$; $n=3$) after normalization to Gapdh. (F) Confocal images of C-
8 HyP (red) and Protein disulphide isomerase (PDI; green) immunofluorescence on ESCs \pm L-Pro
9 (*left*). Half circles indicate Endoplasmic reticulum (ER). Quantification of C-HyP intensity
10 (*right*). Data are mean \pm SD ($*p\leq 0.001$; $n=3$). (G) Western blot analysis of Colla1 in ESCs + L-
11 Pro (1mM) \pm Budesonide (10 μ M). Densitometric analysis (ADU) is shown as fold change vs
12 ESCs + L-Pro. Data are mean \pm SEM ($*p\leq 0.01$; $n=3$) after normalization to Gapdh. (H)
13 Fluorescence photomicrographs of Colla1 (green) and confocal images of C-HyP (red)
14 immunofluorescence on L-Pro-treated cells \pm Budesonide. Nuclei are stained with DAPI. (I-J)
15 Western blot analysis of C-HyP in ESCs (I) and PiCs (J) treated with L-Pro (1mM) \pm
16 Budesonide (10 μ M) or VitC (500 μ M). ADU is shown as C-HyP/Gapdh. Data are mean \pm SEM
17 ($*p\leq 0.01$; $n=3$). (K) Schematic representation of L-Pro, VitC and Budesonide effects on C-HyP.

18

19 **Figure 3.** Generation and functional characterization of $P4ha2^{KO}$ and $P4ha2^{KO}/a1^{KD}$ ESCs. (A)
20 RT-PCR of $P4ha2$ from CRISPR-Cas9 Non Targeting (NT) and $P4ha2^{KO}$ ESCs. (B)
21 Representative pictures of Alkaline phosphatase (AP) staining of NT, $P4ha2^{KO}$ and
22 $P4ha2^{KO}/a1^{KD}$ ESC colonies. (C) Western blot analysis of P4ha1 levels in Control (NT),
23 $P4ha2^{KO}/a1^{KD}$ and $P4ha2^{KO}$ ESCs. Anti-Gapdh antibody was used as loading control. (D)

1 Representative photomicrographs (*left*) and colony type quantification (*right*) of colonies
2 generated from NT, *P4ha2^{KO}* and *P4ha2^{KO}/a1^{KD}* ESCs ± L-Pro (500μM) at day 5. Data are
3 mean±SD (**p*<0.01, ~100 colonies scored/condition; n=5). (E) L-Pro -induced proliferation of
4 NT, *P4ha2^{KO}* and *P4ha2^{KO}/a1^{KD}* ESCs ± L-Pro (500μM) analyzed by CCK-8 assay. Data are
5 shown as fold change vs NT minus L-Pro. Data are mean±SEM (**p*<0.01; n=3). (F) Confocal
6 images of C-HyP immunofluorescence on NT, *P4ha2^{KO}* and *P4ha2^{KO}/a1^{KD}* ESCs treated with L-
7 Pro (500μM) (*top*). Nuclei are stained with DAPI. C-Hyp intensity quantification (*bottom*). Data
8 are mean±SD (**p*≤0.01; n=3). (G) Pie graphs comparing the DNA methylation profiles of L-Pro-
9 treated ESCs and the *Tet* triple KO (TKO) ESCs. Blue slices indicate the percentage of hyper-
10 DMRs in TKO that are hypermethylated by L-Pro at day 2 (*top*) and day 5 (*bottom*); *p*-value<10⁻
11 ¹⁶. (H-I) ELISA-based quantification (H) and immunofluorescence (I) of 5hmC in Control (NT),
12 *P4ha2^{KO}* and *P4ha2^{KO}/a1^{KD}* ESCs ± L-Pro (500 μM; 24 hrs). (H) 5hmC levels are shown as fold
13 change vs NT minus L-Pro. Data are mean±SEM (**p*≤0.01; n=3). (I) Fluorescence
14 photomicrographs of 5hmC (red). Nuclei are stained with DAPI. (J-K) Western blot analysis of
15 H3K9me3 in NT, *P4ha2^{KO}* and *P4ha2^{KO}/a1^{KD}* ESCs ± L-Pro (500μM) (J), and in wild-type ESCs
16 ± L-Pro (500μM) ± VitC (K). ADU is shown as fold change vs untreated (minus L-Pro) Controls
17 after normalization to total histone H3. Data are mean±SEM (**p*≤0.01; n=3). (L) Schematic
18 representation of VitC-dependent collagen hydroxylation (P4H) and DNA/Histone hydroxylation
19 (TET/JMJ) in the different subcellular compartments.

20
21 **Figure 4.** Collagen synthesis/hydroxylation induces mesenchymal transition in lung epithelial
22 tumor cells (A549) modifying the epigenetic landscape. (A) Schematic representation of 2D cell
23 migration assay from A549 lung tumor spheroid. (B) Representative photomicrographs of crystal

1 violet stained A549 spheroids treated with Budesonide (10 and 20 μ M) or vehicle (DMSO). (C)
2 Representative pictures of Coll1a1 immunofluorescence on A549 cells treated with Budesonide
3 (10 μ M) or DMSO for 48 hrs. Nuclei are stained with DAPI. (D) Western blot analysis of
4 H3K9me2/me3, H3K27me3, H3K36me3 and H3K4me3 in wild-type A549 cells treated with
5 Budesonide (10 and 20 μ M) or DMSO as control, for 48 hrs. ADU is shown as fold change vs
6 DMSO after normalization to total histone H3. Data are mean \pm SEM (* p \leq 0.01; n=3). (E-G)
7 Generation and functional characterization of *P4HA2^{KD}* A549 cells. (E) Confocal images of C-
8 HyP immunofluorescence on NT and *P4HA2^{KD}* A549 cells (*top*). Nuclei are stained with DAPI.
9 C-Hyp intensity quantification (*bottom*). Data are mean \pm SE (* p \leq 0.01; n=2). (F) Representative
10 photomicrographs of NT and *P4HA2^{KD}* A549 derived spheroids stained with crystal violet (*top*).
11 Quantification of spreading spheroids (*bottom*). Data are mean \pm SE (* p \leq 0.01; n=3). (G) Western
12 blot analysis of H3K9me2 and H3K36me3 in NT and *P4HA2^{KD}* A549 cells. ADU is shown as
13 fold change vs NT after normalization to total histone H3. Data are mean \pm SEM (* p \leq 0.01; n=3).

14

15 **Figure 5.** Collagen prolyl hydroxylation influences the mesenchymal phenotype of triple-
16 negative breast cancer (TNBC) cells modifying the epigenetic landscape. (A) P4HA2 expression
17 is an independent predictor of poor prognosis in Breast Cancer. Left panel: prognostic
18 significance of P4HA2 expression determined by Kaplan-Meier survival analysis in the
19 METABRIC datasets. Right panels: The risk ratios (High vs. Low P4HA2 expression) were
20 estimated with a Cox proportional hazards in univariate and multivariable model, adjusted for
21 standard clinicopathological parameters. (B) Western blot analysis of P4HA2 in Control non-
22 targeted (NT) and *P4HA2^{KD}* SUM159 cells. Anti-GAPDH antibody was used as loading control.
23 (C) Representative pictures of NT and *P4HA2^{KD}* SUM159 cell morphology. (D) Western blot

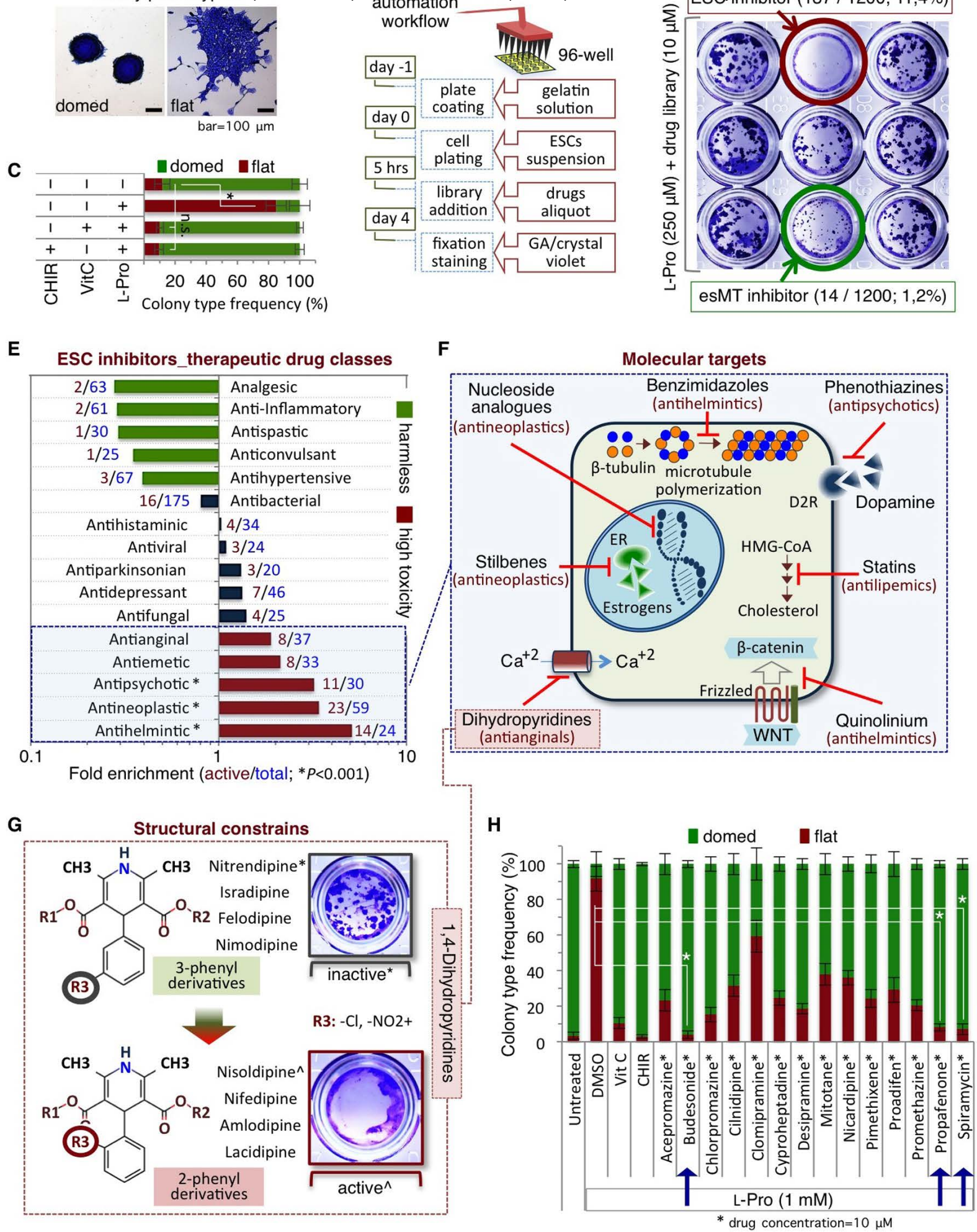
1 analysis of FIBRONECTIN1 (FB1) and VIMENTIN levels in NT and *P4HA2^{KD}* SUM159 cells.
2 Anti-GAPDH antibody was used as loading control. (E) CCK-8 based proliferation assay of NT
3 and *P4HA2^{KD}* SUM159 cells. Data are shown as fold change vs NT and are mean±SEM (n=3).
4 (F) Confocal images of C-HyP immunofluorescence (*left*) and C-Hyp intensity quantification
5 (*right*) of NT and *P4HA2^{KD}* SUM159 cells. Nuclei are stained with DAPI. Data are mean±SE
6 (**p*≤0.01; n=2). (G) Western blot analysis of H3K27me3, H3K36me3, H3K4me3 and
7 H3K9me2/me3 in NT and *P4HA2^{KD}* SUM159 cells. ADU is shown as fold change vs NT after
8 normalization to total histone H3. Data are mean±SEM (**p*≤0.01; n=3).

9
10 **Figure 6.** (A-B) Confocal images of Col1a1 (A) and C-HyP (B) immunofluorescence and signal
11 intensity quantification of wild-type SUM159 cells ± Budesonide (25 μM) for 48 hrs. Nuclei are
12 stained with DAPI. Data are mean±SE (**p*≤0.01; n=3). (C) Western blot analysis of
13 H3K9me2/me3, H3K36me3, and H3K27me3 and H3K4me3 in SUM159 cells ± Budesonide (25
14 μM) for 48 hrs. ADU is shown as fold change vs DMSO after normalization to total histone H3.
15 Data are mean ± SEM (**p*≤0.01; n=3). (D) Western blot analysis of H3K9me2/me3, H3K27me3,
16 H3K4me3 and H3K36me3 in SUM159 cells ± VitC (10, 20 and 50 μM). ADU is shown as fold
17 change vs untreated cells after normalization to total histone H3. Data are mean±SEM (**p*≤0.01;
18 n=3).

19
20 **Figure 7.** Budesonide blocks triple-negative breast cancer cell migration and invasion *in vitro*
21 and *in vivo* (A) Schematic representation of SUM-159 3D organotypic culture assay. (B)
22 Representative pictures (*left*) and circularity index (*right*) of SUM-159-derived spheroids ±
23 Budesonide. The colony circularity was measured by using the formula $\{4\pi \cdot \text{area} / \text{perimeter}^2\}$.

1 A value of 1.0 indicates a perfect circle. As the value approaches to 0.0, it indicates an
2 increasingly elongated shape. Data are mean \pm SD (* $p\leq 0.01$; 50 colonies/group; n=3). (C)
3 Representative pictures of H&E and VIMENTIN staining on sections from SUM-159
4 Luciferase-derived tumors (*left*). Cell circularity (*right*) is shown as mean \pm SD (* $p\leq 0.01$; 50
5 cells/tumors, n=5 mice/group). (D) Representative pictures of Picrosirius red staining and
6 polarized light microscopy of tumor sections (*left*). Collagen quantification is shown as
7 percentage of collagen area/field (*right*). Data are mean \pm SD (* $p\leq 0.01$; n=30 fields/group). (E)
8 Dissemination to lung and distal lymph nodes by *in vivo* imaging in mice \pm Budesonide (*top*). A
9 dark screen was placed on top of the primary tumor to visualize the lower signal of distal foci.
10 The Relative Luciferase counts/mouse (*bottom*) are shown as mean \pm SD (* $p<0.01$; n=5
11 mice/group). (F) Representative pictures of Human Nuclei staining on lung sections from mice \pm
12 Budesonide (*left*). Quantification of disseminated tumor cells is shown as number of
13 micrometastasis/lung (*right*). Data are the mean \pm SD (* $p<0.01$; n=5 mice/group).

14



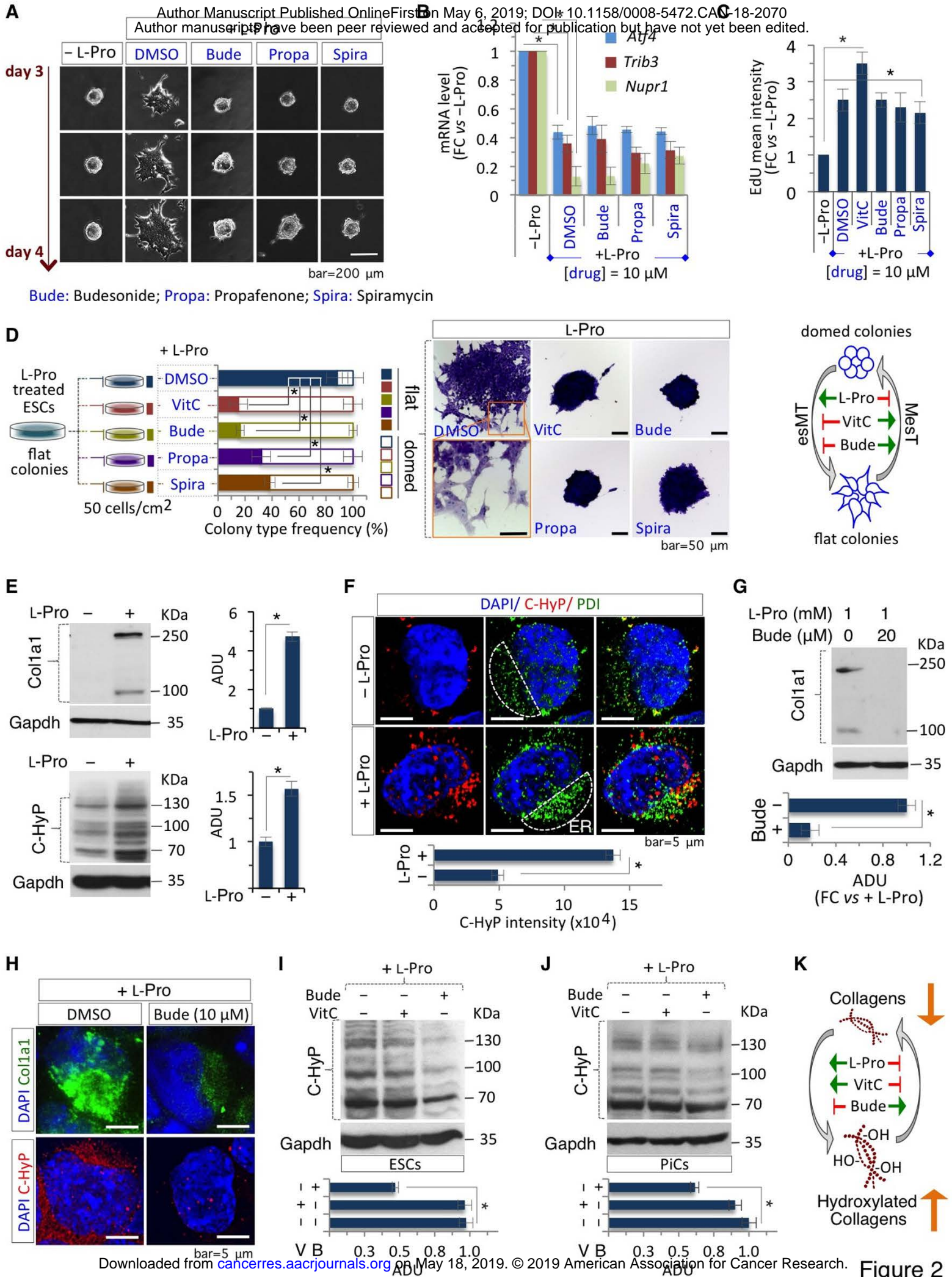
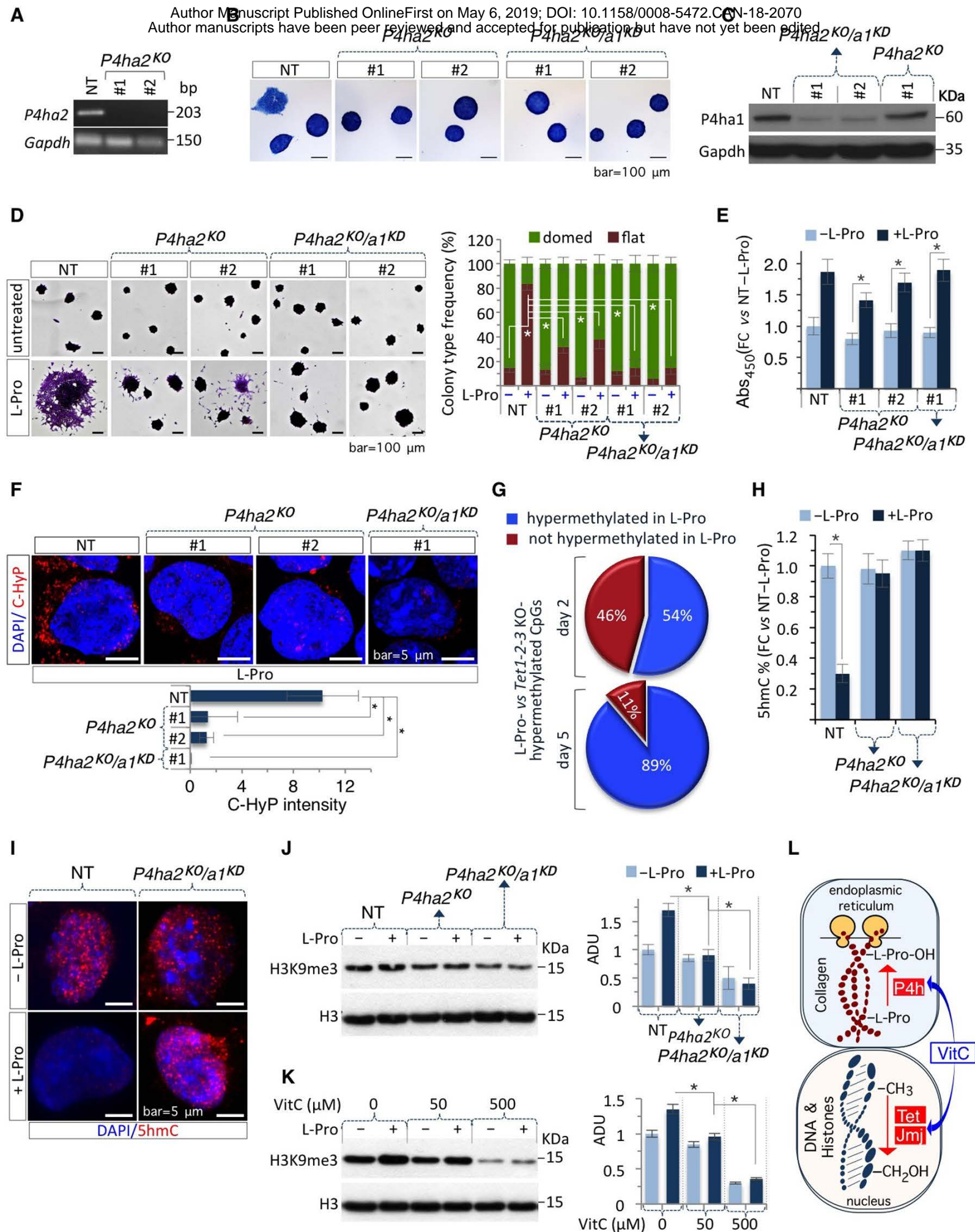


Figure 2



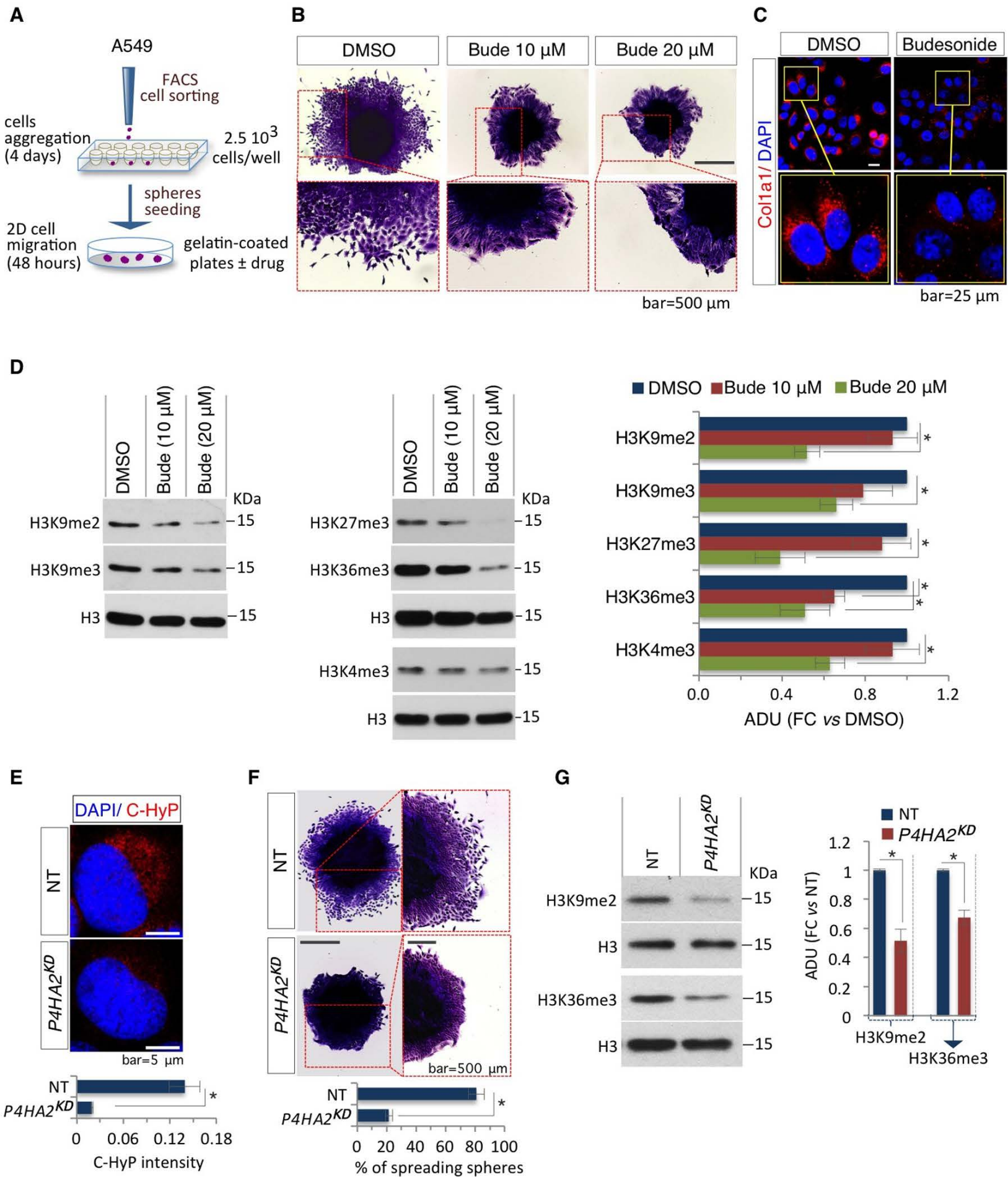


Figure 4

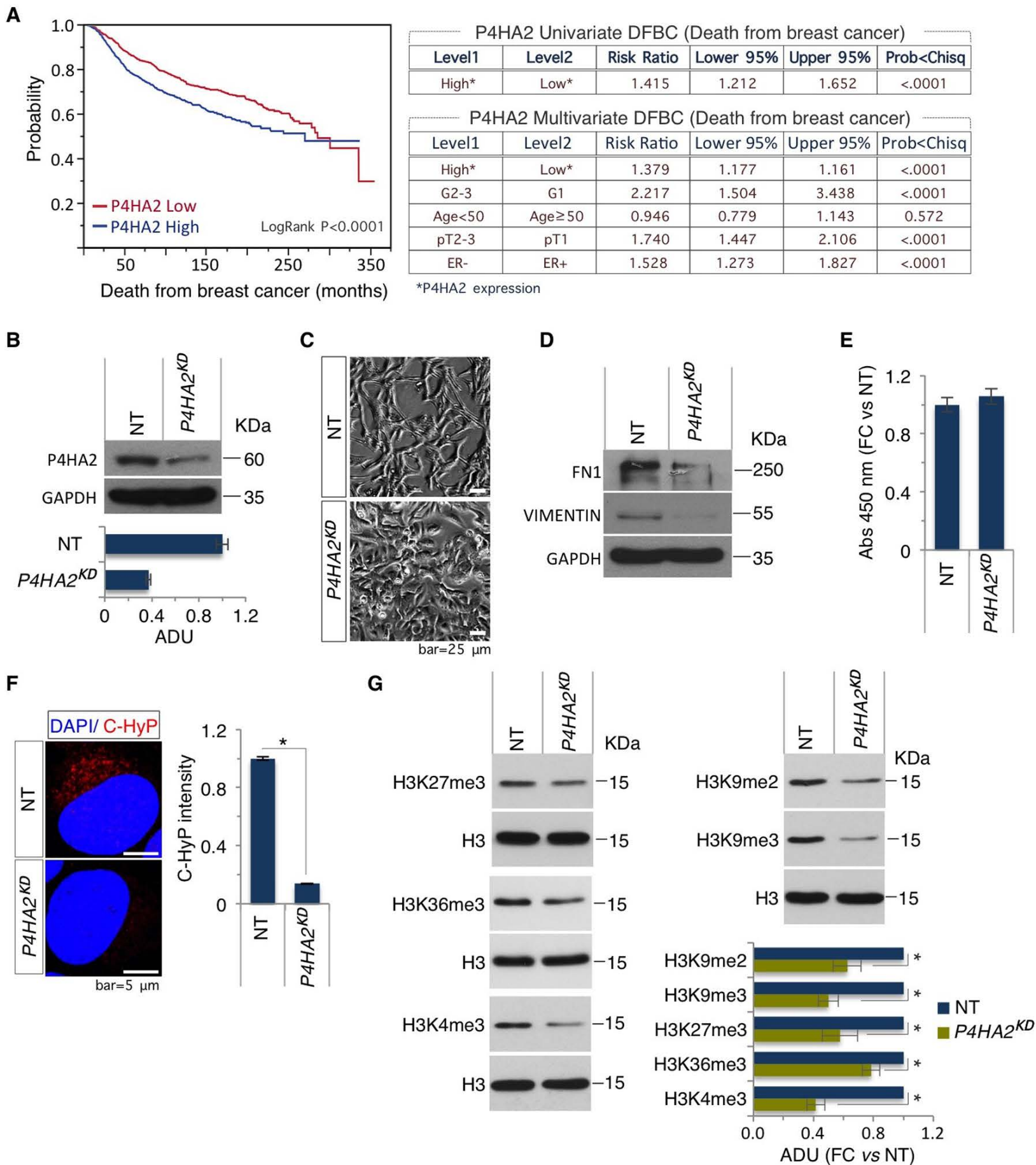


Figure 5

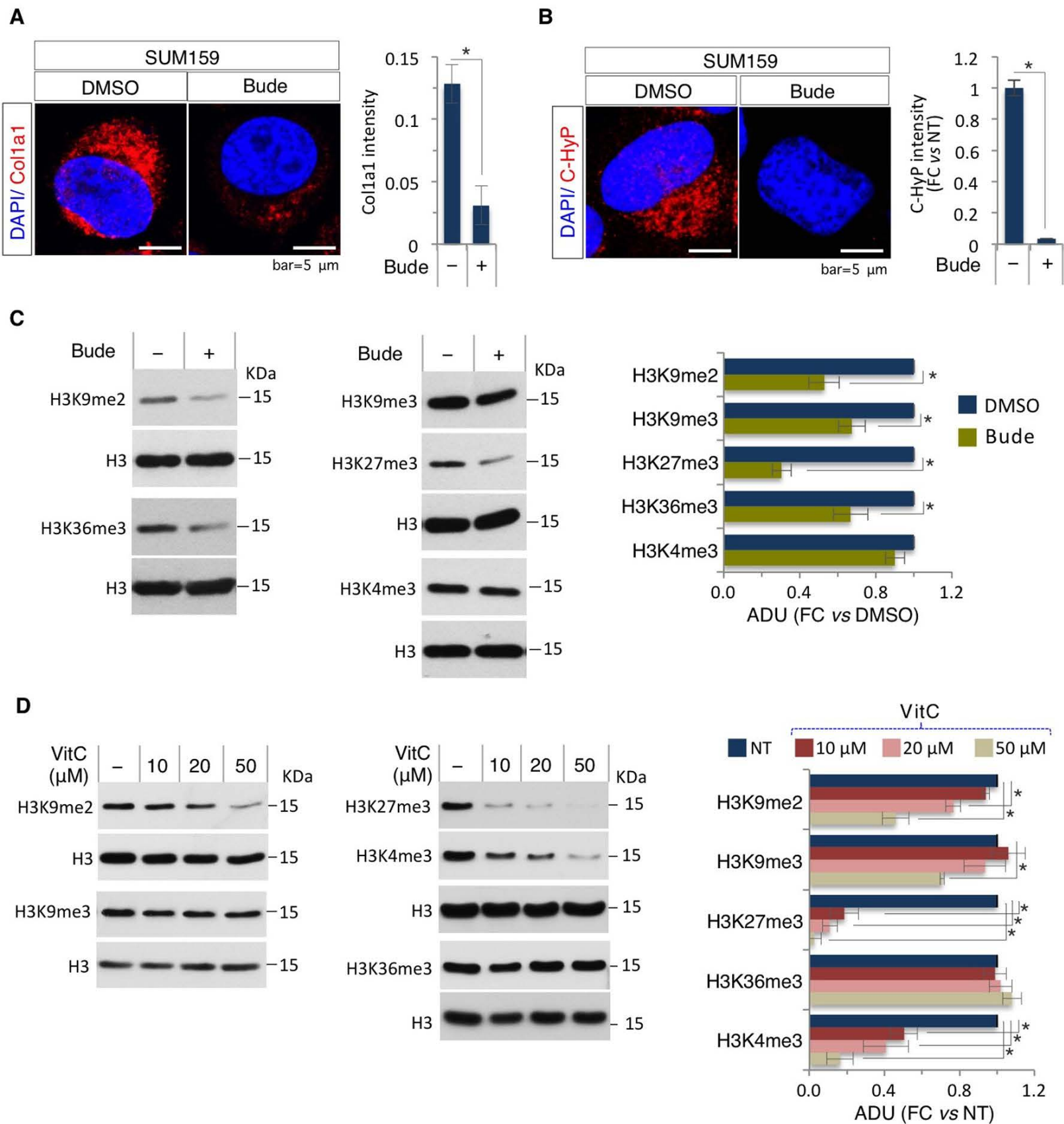


Figure 6

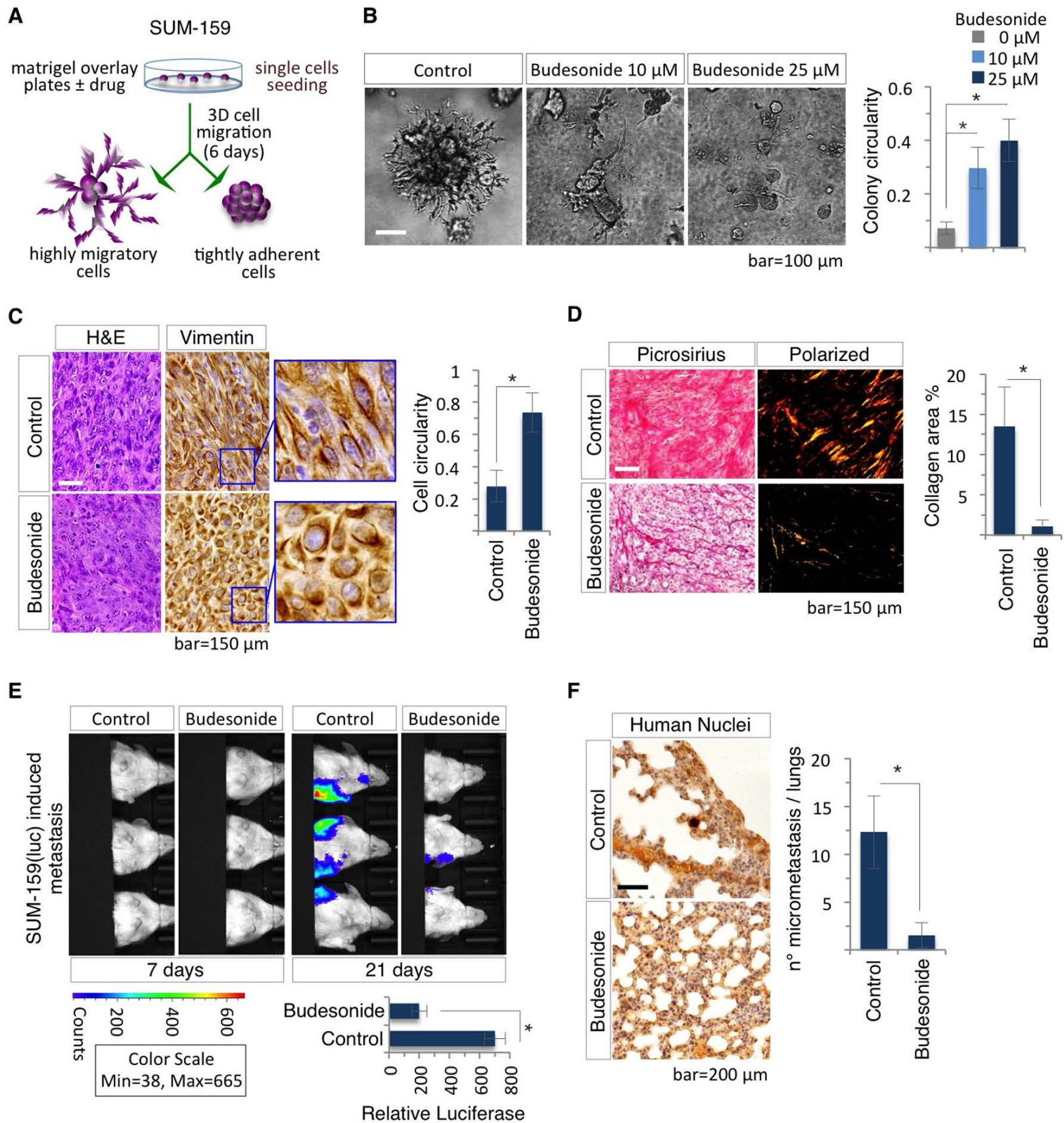


Figure 7

Cancer Research

The Journal of Cancer Research (1916–1930) | The American Journal of Cancer (1931–1940)

Collagen prolyl hydroxylation-dependent metabolic perturbation governs epigenetic remodeling and mesenchymal transition in pluripotent and cancer cells

Cristina D'Aniello, Federica Cermola, Andrea Palamidessi, et al.

Cancer Res Published OnlineFirst May 6, 2019.

Updated version	Access the most recent version of this article at: doi: 10.1158/0008-5472.CAN-18-2070
Supplementary Material	Access the most recent supplemental material at: http://cancerres.aacrjournals.org/content/suppl/2019/05/03/0008-5472.CAN-18-2070.DC1
Author Manuscript	Author manuscripts have been peer reviewed and accepted for publication but have not yet been edited.

E-mail alerts	Sign up to receive free email-alerts related to this article or journal.
Reprints and Subscriptions	To order reprints of this article or to subscribe to the journal, contact the AACR Publications Department at pubs@aacr.org .
Permissions	To request permission to re-use all or part of this article, use this link http://cancerres.aacrjournals.org/content/early/2019/05/03/0008-5472.CAN-18-2070 . Click on "Request Permissions" which will take you to the Copyright Clearance Center's (CCC) Rightslink site.